Inorganic Chemistry

Article

pubs.acs.org/IC

Studies on Polymorphic Sequence during the Formation of the 1:1 Ordered Perovskite-Type $BaCa_{0.335}M_{0.165}Nb_{0.5}O_{3-\delta}$ (M = Mn, Fe, Co) Using in Situ and ex Situ Powder X-ray Diffraction

Wang Hay Kan,[†] Joey Lussier,[‡] Mario Bieringer,[‡] and Venkataraman Thangadurai*,[†]

[†]Department of Chemistry, University of Calgary, 2500 University Drive NW, Calgary, Alberta, Canada T2N 1N4

[‡]Department of Chemistry, University of Manitoba, 144 Dysart Road, Winnipeg, Manitoba, Canada R3T 2N2

Supporting Information

ABSTRACT: Here, we report a synthetic strategy to control the B-site ordering of the transition metal-doped perovskite-type oxides with the nominal formula of $BaCa_{0.335}M_{0.165}Nb_{0.5}O_{3-\delta}$ (M = Mn, Fe, Co). Variable temperature (in situ) and ex situ powder X-ray diffraction (PXRD), selected area electron diffraction (SAED), energy dispersive X-ray spectroscopy (EDX), Fourier transform infrared spectroscopy (FTIR), scanning/transmission electron microscopy (SEM/TEM), and thermogravimetic analysis (TGA) were used to understand the B-site ordering as a function of temperature. The present study shows that $BaCa_{0.335}M_{0.165}Nb_{0.5}O_{3-\delta}$ crystallizes in the B-site disordered primitive perovskite (space group s.g. $Pm\bar{3}m$) at 900 °C in air, which can be converted into the B-site 1:2 ordered perovskite (s.g. $P\bar{3}m1$) at 1200 °C and the B-site 1:1 ordered perovskite phase (s.g. $Fm\bar{3}m$) at 1300 °C. However, the reverse reaction is not feasible when the temperature is reduced. FTIR revealed that no carbonate species were present in all three polymorphs. The chemical stability of the investigated perovskites in CO_2 and H_2 highly depends on the B-site cation ordering. For example, TGA confirmed that the B-site disordered primitive perovskite phase is more readily reduced in dry and wet 10% H_2/90% N_2 and is less stable in pure CO_2 at elevated temperature, compared to the B-site 1:1 ordered perovskite-type phase of the same nominal composition.

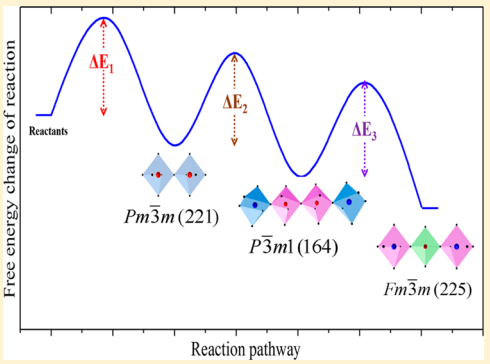

1. INTRODUCTION

Controlling the polymorphs of metal oxides is important but challenging in solid-state chemistry and in materials science. One of the most successful examples is the synthesis of the ceramic dielectric resonator B-site 1:2 ordered perovskite-type $A_3^{2+}B^{2+}M_2^{5+}O_9$ (A = Sr, Ba; B = Co, Zn; M = Nb, Ta).[1−4] The high permittivity value ($\varepsilon_r \approx 30$) is sensitive to the B-site ordering, which is prepared by two-stage solid state synthesis (i.e., 1000 and 1300 °C).[5,6] The initial stage synthesis yields samples with the B-site disordered structure, and the subsequent heat treatment process transforms it into the 1:2 B-site ordering by promoting domain boundary motion and bulk diffusion.[1−3] Another excellent example is the polymorphism of MnO_2 which shows different activities (α- > β- > γ-) toward the oxygen reduction reaction (ORR) in alkaline media for lithium−air batteries.[7,8] The difference in activity arises due to the size of the ions' (H^+, O^{2-}) channels to facilitate the charge transfer reactions: (i) proton insertion, (ii) O_2 adsorption (formation of O_{ads} from O_2), and (iii) electrochemical reduction.[7,8] The formation of various polymorphs may be controlled by the pH-level and the choice of precursors in the low-temperature synthetic methods (e.g., hydrothermal synthesis).

Recently, Demont et al. explored the endotaxial phase separation driven by charge frustration in a complex perovskite-type $Ba_{0.5}Sr_{0.5}Co_{0.8-x}Fe_{0.2-y}Mo_{x+y}O_{3-\delta}$.[9] B-site disordered perovskite-type $Ba_{0.5}Bi_{0.5}Mn_{0.5}Ti_{0.5}O_3$ and $BaCo_{0.5}Nb_{0.5}O_3$ were studied by Norberg and Yoshii.[10,11] Perovskites are among other known metal oxide types being studied intensively for solid oxide fuel cells (SOFCs) because of the high solubility for different dopants at both A- and B-sites and the high structural stability in fuel reducing atmospheres and activity for electrochemical hydrogen oxidation reaction (HOR) and ORR.[12−18] The proton conduction in perovskite is also a popular topic as some mixed conductive perovskites are electrochemically active in ppm of H_2S hydrocarbon fuels C_xH_{2x+2} (x = 1−3).[13] When compared to the simple perovskite-type (space group s.g. $Pm\bar{3}m$),[13,17] the B-site ordered perovskite-type (s.g. $Fm\bar{3}m$) metal oxides are relatively less studied.[19−23] Nonetheless, the B-site ordered perovskite-type structure offers an additional parameter to modify the physical and/or chemical properties through the careful control on dopant substitution on the two different crystallographic B-sites (*4a* and *4b*).[19−21] In the past few years, Irvine, Thangadurai, and Chen groups have focused on the electric properties and defect chemistry of M-doped B-site 1:1 ordered perovskite-type $Ba_3CaNb_{2-x}M_xO_{9-\delta}$ (M = Ti, Mn, Fe, Co, Zn,

Received: March 31, 2014
Published: September 11, 2014

   dx.doi.org/10.1021/ic501270k | *Inorg. Chem.* 2014, 53, 10085−10093

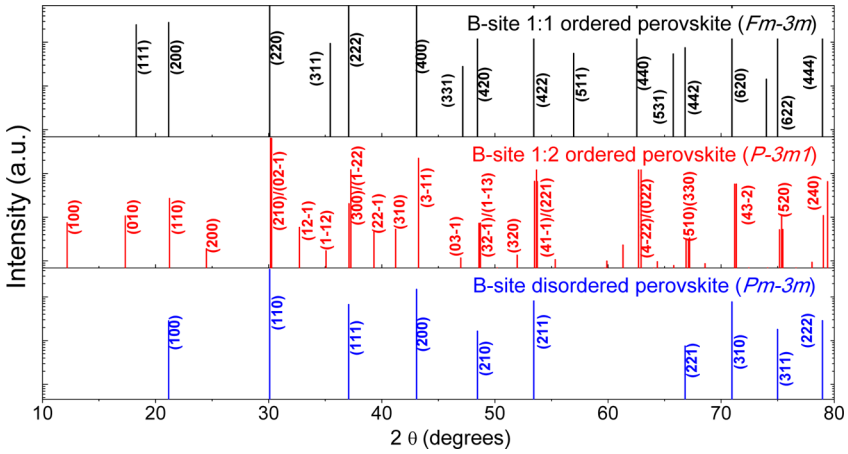

Figure 1. Simulated PXRD patterns of typical B-site disordered, B-site 1:2 ordered and B-site 1:1 ordered perovskites. The crystallographic information files (cif) of $BaCeO_3$ (s.g. $Pm\bar{3}m$; ICSD no. 79628), $Ba_2Ca_{0.67}Nb_{1.33}O_6$ (s.g. $P\bar{3}m1$; ICSD no. 162758), and $Ba_2Ca_{0.79}Nb_{1.21}O_{5.88}$ (s.g. $Fm\bar{3}m$; ICSD no. 93400) were used to simulate the PXRD patterns.

Ta, and Ce).[19−22,24−26] However, it is unclear whether other polymorphs can be stabilized, although the B-site 1:1 ordered perovskite structure was often stabilized at elevated temperature. Different polymorphs could have different solubility of dopants which have strong impact on the temperature-dependent electrical conductivity and electrochemical properties.[7]

Here, we revisited the synthetic procedures and discovered that the B-site disordered primitive perovskite structure with the nominal formula of $BaCa_{0.335}M_{0.165}Nb_{0.5}O_{3-\delta}$ (M = Mn, Fe, Co) was crystallized below 1000 °C. Using variable temperature (in situ) powder X-ray diffraction, we have identified, for the first time, an intermediate metastable phase with the B-site 1:2 ordered perovskite structure, when the B-site disordered perovskite is transformed into the B-site 1:1 ordered perovskite at elevated temperature. The use of sintering temperature as a controlling parameter for the B-site ordering in perovskite materials is rarely studied. In this study, the impact of the B-site ordering on the crystal structure, chemical stability in CO_2, and reducibility in (dry and wet) 10% H_2 in N_2 is systematically studied using state-of-the art solid state methods such as variable temperature powder X-ray diffraction, electron diffraction and thermogravimetric analysis.

2. EXPERIMENTAL SECTION

2.1. Synthesis. $Ba(Ca_{0.335}M_{0.165}Nb_{0.5})O_{3-\delta}$ (M = Mn, Fe, Co) was prepared using stoichiometric amount of $Ba(NO_3)_2$ (99+%, Alfa Aesar), $CaCO_3$ (99%, Fisher Scientific Company), Nb_2O_5 (99.5%, Alfa Aesar), $MnCO_3$ (99+%, Alfa Aesar), Fe_2O_3 (98+%, Alfa Aesar), and $Co(NO_3)_2{\cdot}6H_2O$ (99+%, Fisher Scientific Company) precursors which were ball-milled in the presence of isopropanol at 200 rpm for 12 h in a zirconia bowl. The samples were air-dried at 100 °C before calcinations at 1000 °C for 12 h at the ramp rate of 5 °C/min. The samples were hand-grinded, pelletized isostatically (ca. 200 MPa) and sintered at 1000 °C for 12 h in air. The B-site 1:1 ordered perovskite $Ba_2Ca_{0.67}M_{0.33}NbO_{6-\delta}$ was prepared similarly by premixing the same precursors. The samples were dried at 100 °C and calcined at 1000 °C for 12 h at the ramp rate of 5 °C/min. The samples were repeatedly hand-ground, pelletized isostatically (ca. 200 MPa), and sintered at 1400 °C for 12 h in air, until phase pure samples were obtained.[19−21]

2.2. Phase Characterization. Phases were identified by powder X-ray diffraction (PXRD) (Bruker D8 Advance powder X-ray diffractometer Cu Kα, 40 kV, 40 mA) from 2θ = 10° to 80° at a count rate of 15 s per step of 0.02° at room temperature. For variable temperature (in situ) PXRD (25 to 900 °C), the samples were analyzed in the same Bruker diffractometer with a high temperature reactor chamber (Anton Paar XRK 900) attached. The samples were heated up at the ramp rate of 6 °C/min and then stabilized in the various reactive gases for 30 min, prior to the measurement from 2θ = 10° to 80°, at a count rate of 3 s per step of 0.05°. For in situ PXRD measurement between 1000 to 1300 °C, the samples were analyzed with a PANalytical X'Pert Pro diffractometer equipped with a diffracted beam Ni filter, an X'celerator detector, and an Anton Paar HTK2000 high temperature camera. The measurements were taken from 2θ = 15° to 65°, at a count rate of 45 s per step of 0.0167°. The PXRD data sets were refined by the conventional Rietveld method using the GSAS package with the EXPGUI interface.[27] The background, scale factor, zero-point position, cell parameters, atomic positions, and profile coefficients for Pseudo-Voigt/FCJU Asymmetric peak shape function were refined until the convergence was achieved. Bond lengths were obtained by DISAGL version Win32 Crystal Structure Distance and Angle Program in the GSAS packet on XRD data sets.[27] The bond valences were calculated by Bond Valence Sum Calculator version 2.00.[28]

Iodometic titration was used to determine the oxidation state of transition metals (M) (M = Mn, Fe, Co) ions of the samples and subsequently to determine the oxide ion vacancy of the samples.[19] Such information was used to construct the models for the Rietveld study. The samples were dissolved using HCl and the higher valence transition metal ions can be reduced by KI (e.g., $2I^- + 2Fe^{3+} \rightarrow 2Fe^{2+} + I_2$). The amount of I_2 evolved can be determined using standard $Na_2S_2O_3$ (i.e., $I_2 + 2S_2O_3^{2-} \rightarrow 2I^- + S_4O_6^{2-}$), and starch is used as an indicator. About 0.1 g of the as-prepared sample was dissolved into ca. 15 mL of 4 M HCl on the hot plate at 150 °C for 15 min. The solution was reacted with 10 mL of 20 wt % of KI (ACS-graded, Fisher Scientific company) under an inert atmosphere, and water was used as solvent. The resultant solution was then titrated with standard 0.1 M $Na_2S_2O_3$ (99+%, Alfa Aesar) using a starch solution (ACS-graded, Alfa Aesar) as an indicator under N_2 atmosphere. Each sample was measured three times to confirm the reproducibility.

Selected area electron diffraction (SAED) was performed on a FEI Tecnai F20 FEG-TEM (FEI, Eindhoven, The Netherlands) equipped with a Gatan Imaging Filter and a Gatan 860 GIF 2001 CCD of 1024 × 1024 resolution. Microstructures of the samples were analyzed in a Philips XL 30 conventional scanning electron microscope equipped with an energy dispersive X-ray spectrometer (EDX). Samples were gold-coated prior to prevent the surface charging effect. Images were recorded at 20 kV with a secondary electron detector. Infrared (IR) spectra were recorded in a Varian 7000 FT-IR spectrometer to confirm the absence of carbonate peaks in the bulk samples (ca. 1500−1700 cm^{-1}). The thermal stability measurement was conducted in a Mettler Toledo thermal system TGA/DSC1 (HT 1600) Thermogravimetric

dx.doi.org/10.1021/ic501270k | Inorg. Chem. 2014, 53, 10085−10093

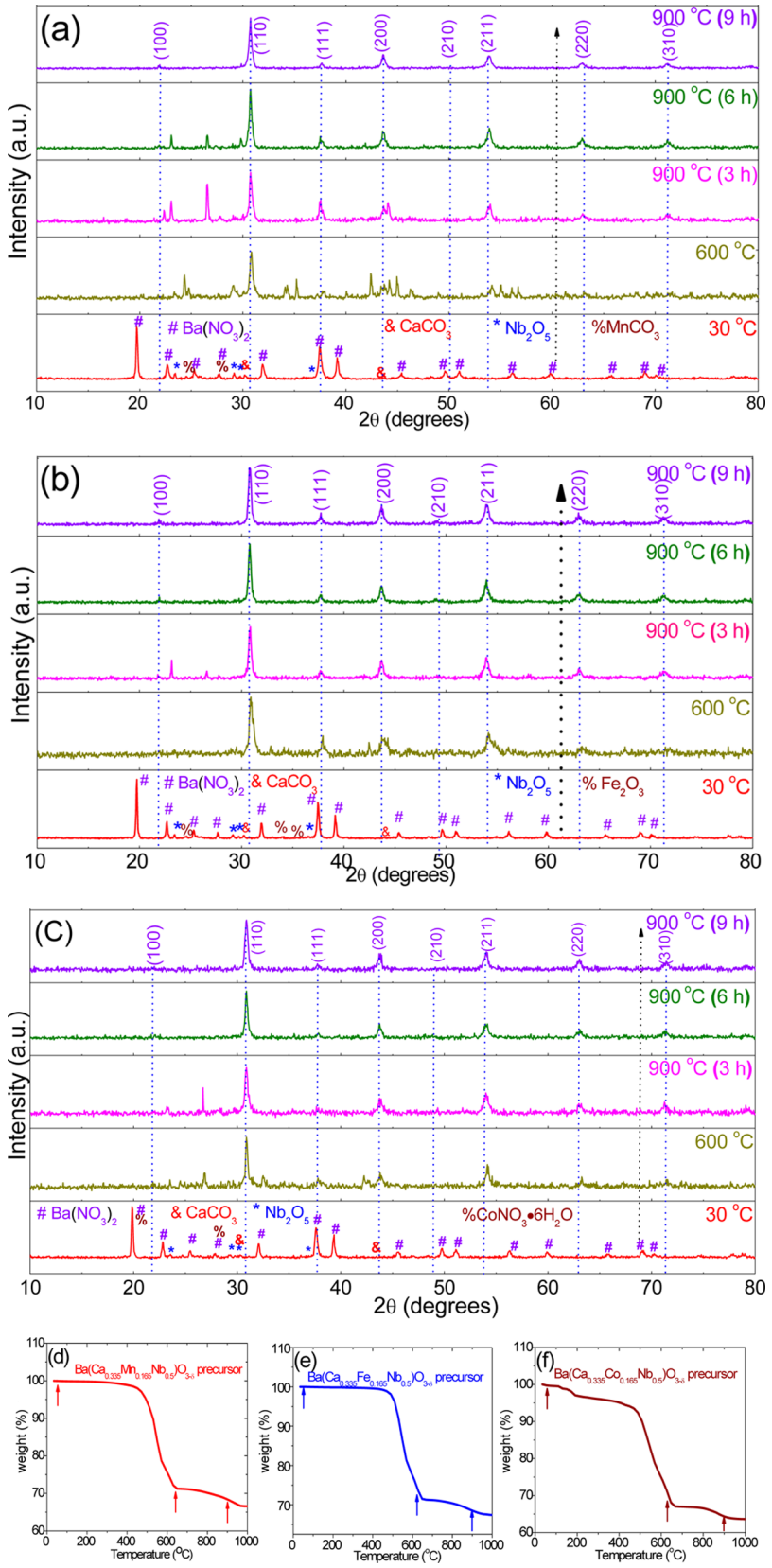

Figure 2. In situ PXRD patterns of the as-mixed reactants as a function of temperature: (a–c) are corresponding to Mn, Fe, Co-doped $BaCa_{0.335}M_{0.165}Nb_{0.5}O_{3-\delta}$ (M = Mn, Fe, Co) samples, respectively. Formation of the B-site disordered perovskite $Ba(Ca_{0.335}M_{0.165}Nb_{0.5})O_{3-\delta}$ was observed at 900 °C. (d–f) are the thermogravimetric analysis (TGA) of the same precursors as a function of temperature. The arrows in the curves indicate the temperatures where the in situ PXRD measurements were taken.

dx.doi.org/10.1021/ic501270k | Inorg. Chem. 2014, 53, 10085–10093

Analyzer with Star^e system. The ramping rate was set to 3 °C/min for both heating and cooling cycles.

3. RESULTS AND DISCUSSION

3.1. Structural Analysis. The stoichiometry-dependent structures of $Ba_3Ca_{1+x}Nb_{2-x}O_{9-\delta}$ have been well studied.[29,30] In

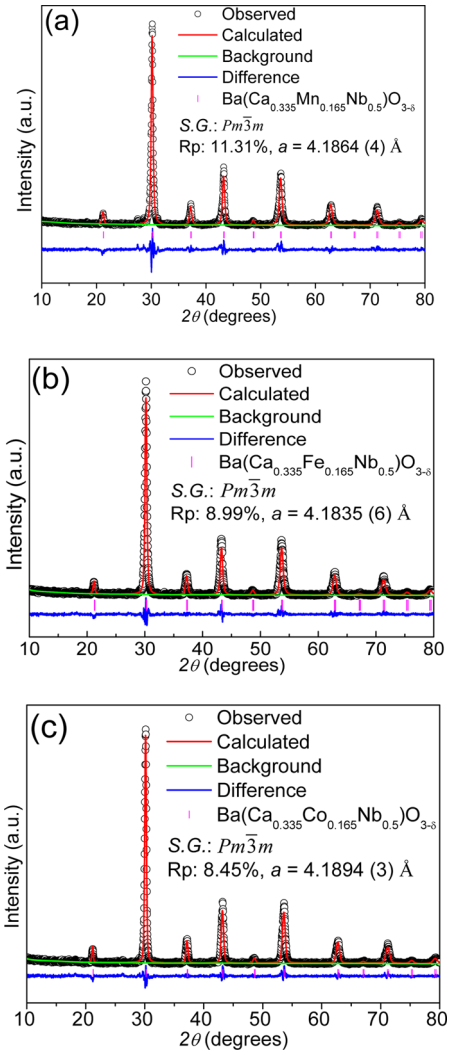

Figure 3. Ex situ PXRD Rietveld refinement of the B-site disordered perovskite $Ba(Ca_{0.335}M_{0.165}Nb_{0.5})O_{3-\delta}$ (M = Mn, Fe, Co) sintered at 1000 °C for 12 h in air. (a), (b), and (c) represent Mn-, Fe-, and Co-doped samples, respectively.

summary, the B-site 1:2 ordered trigonal perovskites, with s.g. $P\bar{3}m1$ (s.g. no. 164), are formed when the Ca/Nb ratio is smaller than 2/3. As the Ca/Nb ratio increases, the B-site 1:1 ordered cubic double perovskites, with s.g. $Fm\bar{3}m$ (s.g. no. 225), are observed. A typical example was the well-known proton conducting $Ba_3Ca_{1.18}Nb_{1.82}O_{9-\delta}$ (BCN18) that was first reported by Nowick et al. in 1994.[29,30] In the unit cell structure of BCN18, both Ca and Nb ions occupy the *4a* sites, while only Nb ions occupy the *4b* sites of the B-site ordered perovskite structure. However, the B-site disordered primitive perovskite structure was not reported for any member with a general formula of $Ba_3Ca_{1+x}Nb_{2-x}O_{9-\delta}$ (x = 0−1). Similarly, many B-site-doped $Ba_3Ca_{1+x-y}Nb_{2-x-z}M_{y+z}O_{9-\delta}$ (M = Ti, Mn, Fe, Co, Zn, Ta, Ce) samples were revealed to have the B-site 1:1 ordered perovskite-type structure.[19−24,31] The above samples were all sintered at an elevated temperature range of 1300−1500 °C in air.

3.2. Polymorphic Sequence during the Formation of the 1:1 Ordered $BaCa_{0.335}M_{0.165}Nb_{0.5}O_{3-\delta}$ Perovskites. The stabilization of different polymorphs with the same nominal formula is an important subject as their chemical and/or physical properties could be different for various applications. Particularly, individual polymorphs could have a distinct solubility limit on dopants with the same size and/or charge, and consequently have a strong impact on the electrical conductivity and catalytic activity.[7] Therefore, we revisited the synthetic route of the B-site 1:1 ordered perovskite-type $Ba_2Ca_{0.67}M_{0.33}NbO_{6-\delta}$ (M = Mn, Fe, Co) and tried to study the temperature-dependent polymorphism.[20,21] The thermodynamically stable B-site 1:1 ordered structured $Ba_2Ca_{0.67}M_{0.33}NbO_{6-\delta}$ is stabilized at elevated temperature,[29,30] while the kinetically stable 1:2 ordered phase might be stabilized at a lower sintering temperature, as suggested by Rosseinsky et al.[1−3] Since different polymorphs have their unique crystal structures and PXRD patterns. One can trace the formation of certain polymorphs through a careful comparison of a series of diffraction peaks. The simulated PXRD patterns of the B-site disordered, the B-site 1:2 ordered, and the B-site 1:1 ordered perovskites are shown in Figure 1. To verify the above hypotheses, the in situ PXRD patterns of the presintered precursor of $Ba_2Ca_{0.67}M_{0.33}NbO_{6-\delta}$ were measured from 25 to 900 °C in air (Figure 2). For the first time, the B-site disordered primitive perovskite-type phase with the nominal formula of $Ba(Ca_{0.335}M_{0.165}Nb_{0.5})O_{3-\delta}$ was observed at 900 °C after 3 hours, albeit, the diffraction peaks were broad and the peak intensities were generally weak and some minor unknown impurities were present.

Thermogravimetic analysis (TGA) revealed that most of the precursors, including $Ba(NO_3)_2$, $CaCO_3$, $MnCO_3$, $Co(NO_3)_2\cdot 6H_2O$, started decomposing at temperatures above 400 °C and contributed to weight losses due to an evolution of gaseous byproducts (i.e., $Ba(NO_3)_{2(s)} \rightarrow BaO_{(s)} + 2NO_{2(g)} + 0.5O_{2(g)}$; $MCO_{3(s)} \rightarrow MO_{(s)} + CO_{2(g)}$, M = Mn, Ca; $Co(NO_3)_2\cdot 6H_2O_{(s)} \rightarrow CoO_{(s)} + 2NO_{2(g)} + 6H_2O_{(g)} + 0.5O_{2(g)}$) (Figure 2(d−f)). The samples were found to be X-ray phase-pure after stabilization at 900 °C for 6 h. The B-site disordered primitive perovskite structure could be well maintained as high as 1000 °C for 12 h. Such ex situ PXRD patterns were selected for a Rietveld refinement study as the diffraction peaks' shape was symmetrical and peak intensities were stronger. A simple model using a primitive cubic unit cell $Pm\bar{3}m$ (s.g. no. 221) was created in which Ba ions were located in the *1a* sites; Ca, dopant (Mn, Fe, and Co) and Nb ions were located in the *1b* sites; oxide ions were located in the *3c* sites. The valence of transition metal M ions in the samples was determined by iodometric titration and was used to calculate the oxide vacancy. The refinement result was plotted in Figure 3, and the structural solution was summarized in Table 1. All diffraction peaks could be well matched with the calculated pattern and small residual values were obtained. The cell parameters of $Ba(Ca_{0.335}M_{0.165}Nb_{0.5})O_{3-\delta}$ are in a range of 4.18−4.19 Å, consistent with other perovskites reported in the literature.[32] However, the cell parameters did not follow Vegard's law, which might be due to the fact that the oxidation states of the dopants changed and possible antisite defects (Figure S1, see the Supporting Information).

The samples were further analyzed by selected area electron microscopy (SAED) to confirm the phase formation. All of the

dx.doi.org/10.1021/ic501270k | Inorg. Chem. 2014, 53, 10085−10093

Table 1. Structural Solution of $BaCa_{0.335}M_{0.165}Nb_{0.5}O_{3-\delta}$ (M = Mn, Fe, Co) Obtained from PXRD Rietveld Refinement Analysis[a]

phase	atom	Wyckoff notation	*x/a, y/b, z/c*	U_{iso} (100 Å^2)	fraction	bond	bond length (Å)	(BVS)
(a) $Ba(Ca_{0.335}Mn_{0.165}Nb_{0.5})O_{2.754}$ $Pm\bar{3}m$ (221), a = 4.1864(4) Å R_p: 11.31, χ^2: 2.324	Ba	*1a*	0,0,0	0.7(1)	1	[Ba−O] × 12	2.9602(2)	1.932
	Ca/Mn/Nb	*1b*	0.5,0.5,0.5	0.3(1)	0.335/0.165/0.5	[Ca/Mn/Nb−O] × 6	2.0932(2)	3.510
	O	*3c*	0.5,0.5,0	1.1(4)	0.918			
(b) $Ba(Ca_{0.335}Fe_{0.165}Nb_{0.5})O_{2.775}$ $Pm\bar{3}m$ (221), a = 4.1835(6) Å R_p: 8.99, χ^2: 1.543	Ba	*1a*	0,0,0	0.15(9)	1	[Ba−O] × 12	2.9582(3)	1.944
	Ca/Fe/Nb	*1b*	0.5,0.5,0.5	0.2(1)	0.335/0.165/0.5	[Ca/Fe/Nb−O] × 6	2.0918(3)	3.472
	O	*3c*	0.5,0.5,0	0.4(3)	0.925			
(c) $Ba(Ca_{0.335}Co_{0.165}Nb_{0.5})O_{2.752}$ $Pm\bar{3}m$ (221), a = 4.1894(3) Å R_p: 8.45, χ^2: 1.600	Ba	*1a*	0,0,0	0.44(9)	1	[Ba−O] × 12	2.9623(2)	1.92
	Ca/Co/Nb	*1b*	0.5,0.5,0.5	0.3(1)	0.335/0.165/0.5	[Ca/Co/Nb−O] × 6	2.0947(2)	3.393
	O	*3c*	0.5,0.5,0	0.6(3)	0.9175			

[a]The bond lengths and bond valence sum (BVS) are included. The valences of Mn, Fe, and Co are 2.05, 2.30 and 2.03, respectively, determined by iodometric titration.

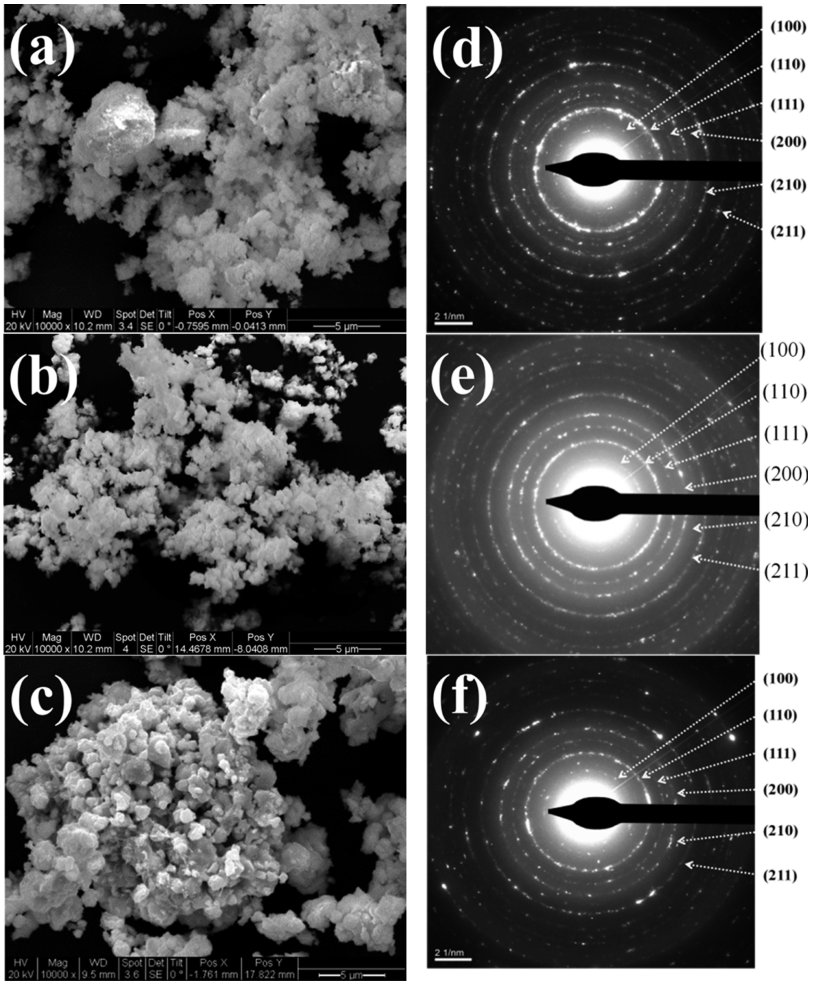

Figure 4. Scanning electron microscopy (SEM) and selected area electron diffraction (SAED) images of the B-site disordered perovskite $Ba(Ca_{0.335}M_{0.165}Nb_{0.5})O_{3-\delta}$ (M = Mn, Fe, Co) sintered at 1000 °C for 12 h. (a) and (d) are Mn; (b) and (e) are Fe; (c) and (f) are Co-doped samples.

Debye rings can be indexed by the same space group and cell parameters, indicating that the samples were phase-pure from grain (SAED) to bulk (PXRD) (Figure 4). The elemental analysis was carried with EDX (Figure S2, see the Supporting Information), and the cationic ratio was consistent with the theoretical ratio. No carbonate species were found in all the investigated $Ba(Ca_{0.335}M_{0.165}Nb_{0.5})O_{3-\delta}$ samples sintered at 1000 °C, further evidenced by the absence of the asymmetric stretching mode of C═O at ca. 1500−1700 cm^{-1} from Fourier transform infrared (FTIR) spectra, as shown in Figure 5.

The B-site disordered primitive perovskite phase is metastable, consequently such a phase should be able to

dx.doi.org/10.1021/ic501270k | *Inorg. Chem.* 2014, 53, 10085−10093

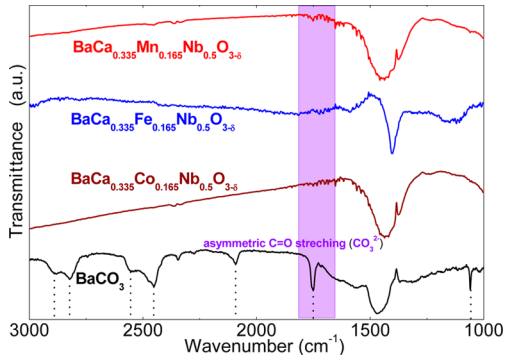

Figure 5. Fourier transform infrared (FTIR) spectra of $BaCa_{0.335}M_{0.165}Nb_{0.5}O_{3-\delta}$ (M = Mn, Fe, Co). There is no indication of carbonate species in all samples, indicated by the purple highlighted region which corresponds to the asymmetric stretching of C═O. The broad peak (1300−1500 cm^{-1}) corresponds to the Ba−O monodentate mode in the perovskite samples. FTIR spectrum of commercial $BaCO_3$ is included for comparison.

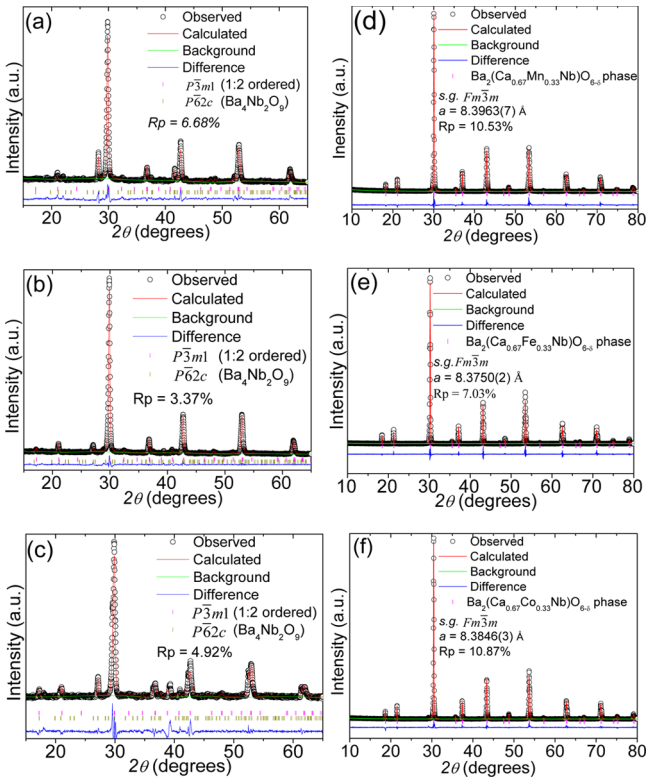

Figure 6. In situ PXRD LeBail refinement of the B-site 1:2 ordered perovskite (s.g. $P\bar{3}m1$) with the nominal formula of $Ba(Ca_{0.335}M_{0.165}Nb_{0.5})O_{3-\delta}$ (M = Mn, Fe, Co) are shown in (a−c). (a), (b), and (c) are Mn (1275 °C), Fe (1275 °C), Co (1225 °C) doped samples, respectively. Small amount of $Ba_4Nb_2O_9$ (s.g. $P\bar{6}2c$) was observed in all samples. The ex situ PXRD Rietveld refinements of the B-site 1:1 ordered perovskite $Ba_2(Ca_{0.67}M_{0.33}Nb)O_{6-\delta}$ (M = Mn, Fe, Co) are shown in (d−f).

transform into thermodynamic stable phases as the temperature increased.[1−3] We tried to understand this process by measuring the variable temperature PXRD patterns in a temperature range between 1000 and 1300 °C. In an attempt to capture all kinetic phases in the heating process, the samples were scanned in 20 min intervals. Surprisingly, diffraction peaks due to the trigonal B-site 1:2 ordered perovskite phase was observed at ca. 1200 °C. The corresponding PXRD patterns were fitted using LeBail refinement and s.g. $P\bar{3}m1$ was found to match well with most diffraction peaks (Figure 6a−c). A small amount of impurity phase of $Ba_4Nb_2O_9$ (s.g. $P\bar{6}2c$) was also observed for all samples. The residue value in the LeBail refinement was found to be 2−3% smaller when the impurity phase of $Ba_4Nb_2O_9$ was included. The refined cell volume (V = 801 to 805 $Å^3$) of $Ba_4Nb_2O_9$ in all samples was found to be slightly bigger than the value (V = 800 $Å^3$) in ICSD database recorded at ambient condition. Such larger cell volumes could be caused by the thermal expansion of the unit cells at elevated temperature. As temperature increased further, the trigonal B-site 1:2 ordered perovskite phase ($P\bar{3}m1$) was found to convert into the cubic B-site 1:1 ordered perovskite phase ($Fm\bar{3}m$) in the isothermal in situ PXRD pattern at 1300 °C (Figure 7).

One of the most characteristic peaks for $P\bar{3}m1$ phase is the (010) diffraction peak at ca. 2θ = 17.1°, while the $Fm\bar{3}m$ phase can be probed by the (111) diffraction peak at ca. 2θ = 18.1°.[29,30] The integrated areas of (010) for the space group $P\bar{3}m1$ and (111) for the $Fm\bar{3}m$ phases were analyzed isothermally at 1300 °C as a function of time (Figure 8). It is interesting to see that the (010) peak area was decreasing and (111) peak area was increasing with increasing sintering time (Figure 8). The full conversion for the B-site 1:2 ordered to the B-site 1:1 ordered phases did not happen at 1300 °C, but it was observed at 1400 °C. The B-site 1:1 ordered perovskite phase has three additional diffraction peaks from (111), (113), and (331) planes for s.g. $Fm\bar{3}m$ (no. 225) at 2θ = ca. 18.5°, 35.4°, and 46.9° respectively, due to the complete B-site ordering. The ex situ PXRD Rietveld refinement patterns of the B-site ordered M-doped $Ba_2(Ca_{0.67}M_{0.33}Nb)O_{6-\delta}$ are shown in Figure 6d−f. The structural solution for the B-site 1:1 ordered perovskite $Ba_2(Ca_{0.67}M_{0.33}Nb)O_{6-\delta}$ was reported in our earlier paper.[19] Although, different phases were observed when the precursors were heated as a function of temperature, the reverse reaction was not feasible. A schematic diagram of the phase conversion as a function of reaction pathway is shown in Figure 9. The cell parameter and space group of $Ba(Ca_{0.335}M_{0.165}Nb_{0.5})O_{3-\delta}$ at different temperatures were summarized in S. Table 1 (see the Supporting Information).

3.3. Effect of B-Site Ordering on Chemical Stability in CO_2 and in 10% H_2 in N_2. Several B-site disordered perovskites, such as $BaCeO_3$ and $BaCe_{1-x}Ln_xO_{3-\delta}$, are susceptible to form $BaCO_3$ and other oxides in CO_2 atmosphere at elevated temperature.[32,33] Small amount of Zr dopant substituted for Ce are found to effectively improve the chemical stability of the compounds under CO_2 at elevated temperatures.[33] Interestingly, some double perovskites, such as BCN18, are chemically stable under the same condition.[29,30] However, it is still unclear whether their chemical composition and/or the B-site ordering play a role in determine the chemical properties. Ideally, one could compare the chemical stability in CO_2 for two different B-site ordered compounds with the same nominal chemical formula, but it is technically challenging. We tried to answer the question by comparing the chemical stability in CO_2 at elevated temperatures for the B-site disordered $Ba(Ca_{0.335}M_{0.165}Nb_{0.5})O_{3-\delta}$ and the B-site 1:1 ordered double perovskite $Ba_2(Ca_{0.67}M_{0.33}Nb)O_{6-\delta}$. We were also interested in studying the chemical stability for the B-site 1:2 ordered perovskites. However, such a phase can only be observed in situ at elevated temperature, and is difficult to isolate for further study.

dx.doi.org/10.1021/ic501270k | Inorg. Chem. 2014, 53, 10085−10093

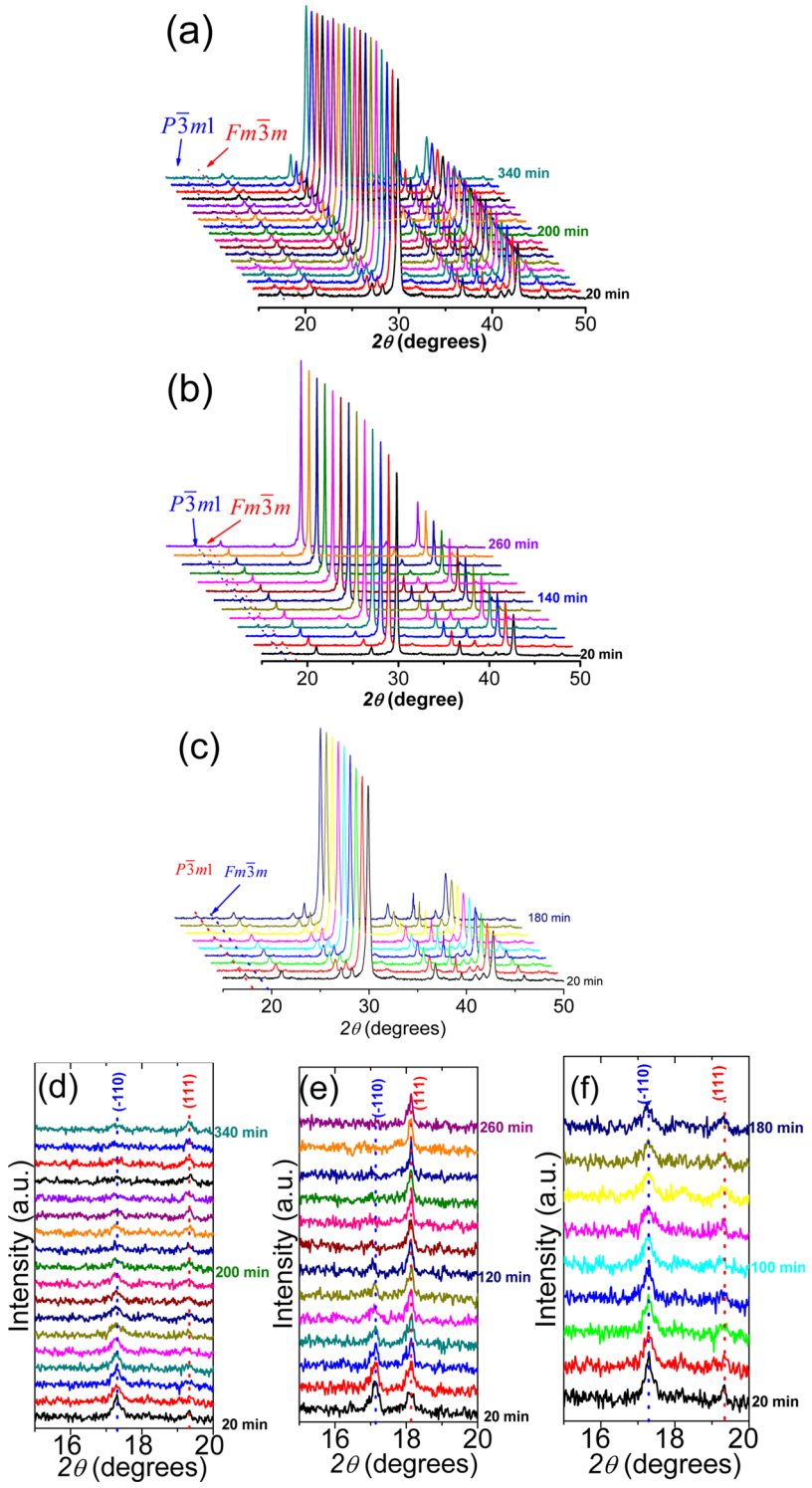

Figure 7. In situ PXRD patterns of the formation of the B-site 1:1 ordered perovskite phase ($Fm\bar{3}m$) were observed at 1300 °C as a function of time (20 min per scan).

In our TGA analysis, we observed a small weight gain for $Ba(Ca_{0.335}M_{0.165}Nb_{0.5})O_{3-\delta}$ with the B-site disordered primitive structure in the temperature range 600−1000 °C under CO_2. We suspected that it was due to the formation of $BaCO_3$ (i.e., $BaO_{(s)} + CO_{2(g)} \rightarrow BaCO_{3(s)}$).[33] The weight gain for Mn- and Fe-doped samples are comparable, while the Co-doped samples showed the highest (Figure 10a) weight gain. On the other hand, the sample with the B-site 1:1 ordered perovskite structure showed small weight loss likely due to the loss of oxygen molecules when Mn, Fe, and Co ions were partially reduced (i.e., $2M^{n+1}{}_{(s)} + O^{2-}{}_{(s)} \rightarrow 2M^{n+}{}_{(s)} + 1/2O_{2(g)}$) (Figure 10d).[33]

The B-site disordered perovskite structure is often reported to have a higher conductivity than the B-site ordered perovskite analogue in air, N_2 and H_2.[34] For example, the oxide-ion conductivity of acceptor-doped $BaCe_{0.9}Y_{0.1}O_{3-\delta}$ is reported to be on the order of 10^{-1} S cm^{-1} in air at 800 °C,[32] while the B-site 1:1 ordered perovskite BCN18 exhibits conductivity on the

dx.doi.org/10.1021/ic501270k | Inorg. Chem. 2014, 53, 10085−10093

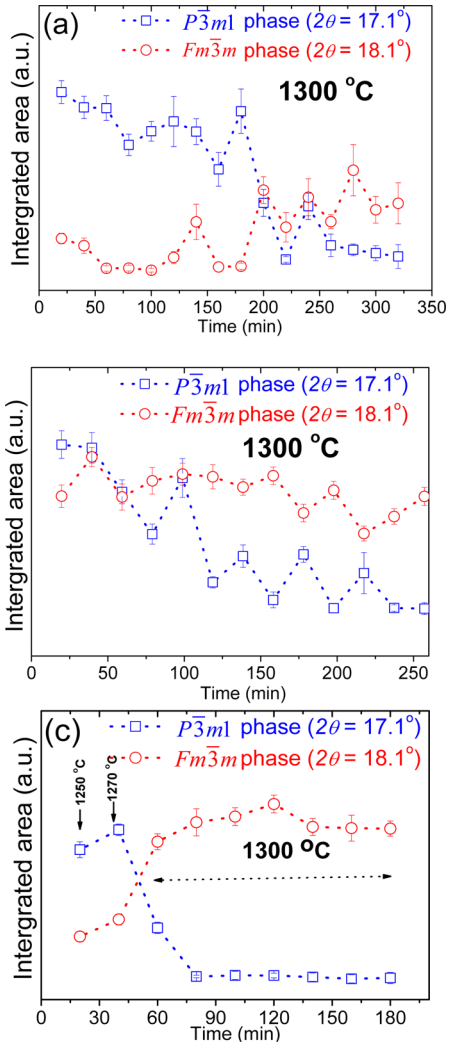

Figure 8. Solid phase conversion of the B-site 1:2 ordered perovskite (s.g. $P\bar{3}m1$) into the B-site 1:1 order perovskite (s.g. $Fm\bar{3}m$) was directly observed in in situ PXRD. The integrated peak areas of $P\bar{3}m1$ (2θ = 17.1°) and $Fm\bar{3}m$ (2θ = 18.1°) were analyzed as a function of time at a constant temperature. (a), (b), and (c) are Mn-, Fe-, and Co-doped samples, respectively. For Co-doped sample, the $P\bar{3}m1$ phase was not observed after 180 min. Therefore; the peak area after 180 min was not included.

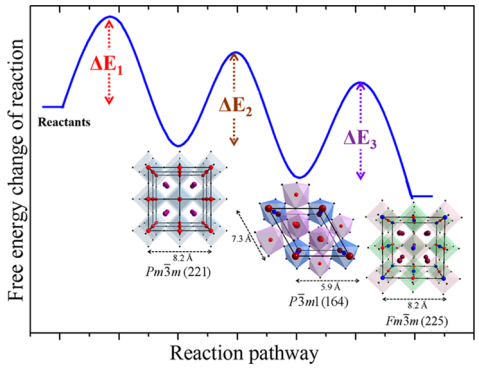

Figure 9. Schematic diagram shows the change of free energy of the reaction of the precursors, the metastable B-site disordered primitive perovskite phase, the B-site 1:2 ordered perovskite phase and the B-site 1:1 ordered perovskite phase.

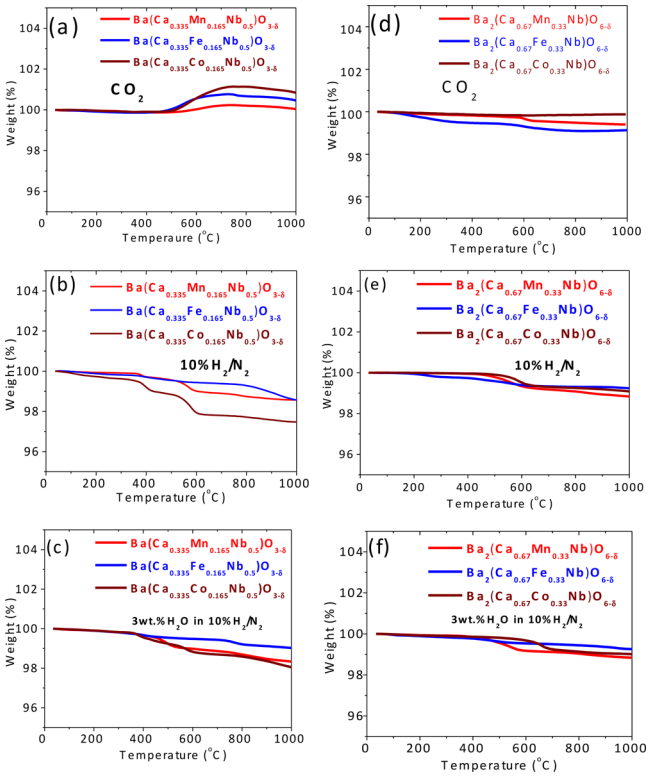

Figure 10. Thermogravimetic analysis (TGA) of the B-site disordered primitive perovskite phase $Ba(Ca_{0.335}M_{0.165}Nb_{0.5})O_{3-\delta}$ (M = Mn, Fe, Co) and the B-site ordered double-perovskite phase $Ba_2(Ca_{0.67}M_{0.33}Nb)O_{6-\delta}$ (M = Mn, Fe, Co) in pure CO_2 (a, d), dry 10% H_2 in N_2 (b, e), and 3 wt % H_2O (c, f) in 10% H_2 in N_2 are compared.

order of 10^{-2} S cm^{-1}, at the same temperature.[29,30] In the presence of water vapor, the conductivity of both phases increases up to 10^{-1} S cm^{-1} due to the contribution of hydroxyl proton conduction (i.e., $V_O^{\bullet\bullet} + O_O^x + H_2O_{(g)} \rightarrow 2OH_O^{\bullet}$; where $V_O^{\bullet\bullet}$, O_O^x, and $OH_O^{\bullet}$ represent oxide ion vacancies, lattice oxygen, and proton attached to lattice oxygen, respectively). We analyzed the samples using a TGA in both dry and wet (3% H_2O) in 10% H_2 in N_2. Interestingly, we found that the B-site disordered primitive perovskite phase had more weight loss in 10% H_2 in N_2 from 30 to 1000 °C than the B-site 1:1 ordered perovskite phase, and it was consistent with the literature proceeding.[32,33] (Figure 10b,c,e,f). The difference was more noticeable in a temperature range between 600 and 1000 °C. In the same atmospheres, Mn- and Co-doped samples are more readily reduced than the Fe-doped samples for both the B-site disordered and ordered perovskite phases. The weight losses in both dry and wet 10% H_2 in N_2 are similar, suggesting that the concentrations of $OH^{\bullet}$ hydroxyl ions in both phases are not significant for proton conduction.[19,32,33] For the B-site disordered primitive perovskite phase, we could not densify the samples by a conventional ceramic method at 1000 °C or lower (to maintain the phase), and therefore, its conductivity could not be addressed in relation to the B-site ordered phase.

4. CONCLUSIONS

In summary, we report a synthetic strategy to control the B-site ordering of Fe-doped perovskites with the nominal formula of $BaCa_{0.335}M_{0.165}Nb_{0.5}O_{3-\delta}$ (M = Mn, Fe, Co) which crystallized into the B-site disordered primitive perovskite phase at 900 °C

dx.doi.org/10.1021/ic501270k | Inorg. Chem. 2014, 53, 10085−10093

in air. The B-site disordered primitive perovskite-type $BaCa_{0.335}M_{0.165}Nb_{0.5}O_{3-\delta}$ can be converted into the B-site 1:2 ordered perovskite at 1200 °C and the B-site 1:1 ordered perovskite phase at 1300 °C in air. The ordering at the B-site is found to increase with temperature and the B-site ordered 1:1 double perovskite phase is observed at 1400 °C in air. FTIR revealed that no carbonate species were present in $Ba(Ca_{0.335}M_{0.165}Nb_{0.5})O_{3-\delta}$. The B-site ordered perovskite-type phase showed higher structural stability in pure CO_2, compared to the B-site disordered phase at elevated temperatures. TGA confirmed that the B-site disordered primitive perovskite phase had higher reducibility in both dry and wet 10% H_2 in N_2, compared to the B-site 1:1 ordered perovskite phase. Under the same condition, Mn- and Co-doped perovskite samples are more readily reduced than the Fe-doped samples.

■ ASSOCIATED CONTENT

Ⓢ Supporting Information

The cell parameter and energy dispersive X-ray spectra (EDX) of the B-site disordered $Ba(Ca_{0.33}M_{0.165}Nb_{0.5})O_{3-\delta}$ (M = Mn, Fe, Co). This material is available free of charge via the Internet at http://pubs.acs.org.

■ AUTHOR INFORMATION

Corresponding Author

*Phone 1 403 210 8649. E-mail: vthangad@ucalgary.ca.

Notes

The authors declare no competing financial interest.

■ ACKNOWLEDGMENTS

This research was supported through funding by the NSERC Solid Oxide Fuel Cell Canada Strategic Research Network from the Natural Science and Engineering Research Council (NSERC) and other sponsors listed at www.sofccanada.com. W.H.K. thanks the Alberta Innovates − Technology Futures (AITF) for nanotechnology graduate student scholarship. We thank the Canada Foundation for Innovation (CFI) for providing funding for the X-ray facility. We thank Professor Todd Sutherland in the Department of Chemistry, University of Calgary for using his FTIR instrument.

■ REFERENCES

(1) Mallinson, P. M.; Claridge, J. B.; Rosseinsky, M. J.; Ibberson, R. M.; Wright, J. P.; Fitch, A. N. *Chem. Mater.* **2007**, *19*, 4731−4740.
(2) Moussa, S. M.; Ibberson, R. M.; Bieringer, M.; Fitch, A. N.; Rosseinsky, M. J. *Chem. Mater.* **2003**, *15*, 2527−2533.
(3) Mallinson, P. M.; Claridge, J. B.; Rosseinsky, M. J.; Ibberson, R. M.; Wright, J. P.; Fitch, A. N.; Price, T.; Iddles, D. M. *Appl. Phys. Lett.* **2007**, *91*, 222901/1−222901/3.
(4) Treiber, U.; Kemmler-Sack, S. *J. Solid State Chem.* **1982**, *43*, 51−62.
(5) Kawashima, S.; Nishida, M.; Ueda, I.; Ouchi, H. *J. Am. Ceram. Soc.* **1983**, *66*, 421−423.
(6) Sagala, D. A.; Nambu, S. *J. Am. Ceram. Soc.* **1992**, *75*, 2573−2575.
(7) Cheng, F.; Chen, J. *Chem. Soc. Rev.* **2012**, *41*, 2172−2192.
(8) Cheng, F.; Su, Y.; Liang, J.; Tao, Z.; Chen, J. *Chem. Mater.* **2010**, *22*, 898−905.
(9) Demont, A.; S, R.; Tsiamtsouri, M. A.; Romani, S.; Chater, P. A.; Niu, H.; Marti-Gastaldo, C.; Xu, Z.; Deng, Z.; Breard, Y.; Thomas, M. F.; Claridge, J. B.; Rosseinsky, M. J. *J. Am. Chem. Soc.* **2013**, *135*, 10114−10123.
(10) Norberg, S. T.; H, S.; Mathieu, R.; Eriksson, S. G. *Chem. Commun.* **2010**, *46*, 1455.
(11) Yoshii, K. *J. Solid State Chem.* **2000**, *151*, 294−297.
(12) Huang, Y.-H.; Dass, R. I.; Xing, Z.-L.; Goodenough, J. B. *Science* **2006**, *312*, 254−257.
(13) Yang, L.; Wang, S.; Blinn, K.; Liu, M.; Cheng, Z.; Liu, M. *Science* **2009**, *326*, 126−129.
(14) Murray, E. P.; Tsai, T.; Barnett, S. A. *Nature* **1999**, *400*, 649−651.
(15) Park, S.; Vohs, J. M.; Gorte, R. J. *Nature* **1999**, *404*, 265−267.
(16) Zhan, Z. I.; Barnett, S. A. *Science* **2005**, *308*, 844−847.
(17) Atkinson, A.; Barnett, S.; Gorte, R. J.; Irvine, J. T. S.; McEvoy, A. J.; Mogensen, M.; Singhal, S. C.; Vohs, J. *Nat. Mater.* **2004**, *3*, 17−27.
(18) Tao, S.; Irvine, J. T. S. *Nat. Mater.* **2003**, *2*, 320−323.
(19) Kan, W. H.; Roushanafshar, M.; Vincent, A.; Fürstenhaupt, T.; Parvez, M.; Luo, J.; Thangadurai, V. *RSC Adv.* **2013**, *3*, 23824−23832.
(20) Kan, W. H.; Trang, T. T.; Fürstenhaupt, T.; Thangadurai, V. *ECS Trans.* **2011**, *35*, 1259−1266.
(21) Kan, W. H.; Trang, T. T.; Fürstenhaupt, T.; Thangadurai, V. *Can. J. Chem.* **2011**, *89*, 688−696.
(22) Viana, H. D. A. L.; Irvine, J. T. S. *J. Mater. Chem.* **2010**, *20*, 8506−8511.
(23) Wang, S.; Zhao, F.; Zhang, L.; Brinkman, K.; Chen, F. *J. Power Sources* **2011**, *196*, 7917−7923.
(24) Trang, T. T.; Thangadurai, V. *Electrochim. Acta* **2010**, *56*, 227−234.
(25) Wang, S.; Zhao, F.; Zhang, L.; Brinkman, K.; Chen, F. *J. Power Sources* **2011**, *196*, 7917−7923.
(26) Bhella, S. S.; Thangadurai, V. *J. Power Sources* **2009**, *186*, 311−319.
(27) Toby, B. H. *J. Appl. Crystallogr.* **2001**, *34*, 210−213.
(28) Brown, I. D.; Altermatt, D. *Acta Crystallogr.* **1985**, *B41*, 244−247.
(29) Liang, K. C.; Du, Y.; Nowick, A. S. *Solid State Ionics* **1994**, *69*, 117−120.
(30) Liang, K. C.; Nowick, A. S. *Solid State Ionics* **1993**, *61*, 77−81.
(31) Thangadurai, V.; Kan, W. H.; Mirfakhraei, B.; Bhella, S. S.; Trinh, T. T. *ECS Trans.* **2011**, *35*, 483−492.
(32) Iwahara, I.; Esaka, T.; Uchida, H.; M, N. *Solid State Ionics* **1981**, *3*−*4*, 359−363.
(33) Fabbri, E.; Pergolesi, D.; Traversa, E. *Chem. Soc. Rev.* **2010**, *39*, 4355−4369.
(34) DeCaluwe, S. C.; Grass, M. E.; Zhang, C.-J.; Gabaly, F. E.; Bluhm, H.; Liu, Z.; Jackson, G. S.; McDaniel, A. H.; McCarty, K. F.; Farrow, R. L.; Linne, M. A.; Hussain, Z.; Eichhorn, B. W. *J. Phys. Chem. C* **2010**, *114*, 19853−19861.